

BedDot: Continuous Contactless Sleep and Vital Signs Monitoring

Yingjian Song, Bingnan Li, Dan Luo, Bradley G. Phillips, Yuan Ke, and Wenzhan Song
The University of Georgia

Abstract—In this paper, we introduce BedDot, a geophone-based contactless vital signs monitoring system designed for continuous monitoring during sleep, as well as adaptation to seats. While many existing contactless vital signs monitoring solutions focus solely on calculating vital signs from well-collected datasets, they do not address the challenge of automatically detecting bed occupancy and obtaining high-quality data to accurately estimate vital signs in contactless systems. Additionally, few studies have explored geophone-based contactless vital signs estimation on both bed and seat. To address these challenges, we propose a signal quality assessment algorithm consisting of three parts: bed occupancy detection, movement detection, and heartbeat detection, to identify high-quality data. We also develop a series of vital signs estimation algorithms that leverage the Bayesian theorem for contactless heart rate (HR), respiration rate (RR), and inter-beat interval (IBI) estimation. Our experimental results demonstrate that our system achieves over 99% accuracy for bed occupancy detection, and MAE of 1.08 BPM, 1.54 BPM, and 24.81 ms for HR, RR, and IBI estimation, respectively, compared with an FDA-approved device. Our system has been extensively tested with data collected from 75 subjects for more than 80 hours under different conditions, demonstrating its generalizability across different people and environments. With its potential for commercialization in both home and hospital use, BedDot is a promising solution for contactless vital signs monitoring.

Index Terms—Contactless Monitoring, Vital Signs, heart rate, respiratory rate, inter-beat interval, sleep, bed occupancy

I. INTRODUCTION

Monitoring vital signs such as heart rate (HR), respiratory rate (RR), and inter-beat interval (IBI) during sleep is important, especially for elder people and children. For example, monitoring HR can predict and even prevent heart failure during sleep. In addition, sleep apnea can be identified by

Yingjian Song and Wenzhan Song are with the School of Electrical and Computer Engineering, University of Georgia, Athens, GA 30602 USA. (e-mail: yingjian.song@uga.edu, wsong@uga.edu). Wenzhan's research is partially supported by NSF-STTR-1940864, Georgia Research Alliance, DOE-EE0009026, NSF-SaTC-2019311, DOD-FA8571-21-C-0020.

Bradley G. Phillips is with Clinical and Translational Research Unit, University of Georgia, Athens, GA 30602 USA. (e-mail: bgp@uga.edu). Bradley's research is partially supported by Georgia CTSA UL1TR002378.

Bingnan Li, Dan Luo and Yuan Ke are with Department of Statistics, University of Georgia, Athens, GA 30602 USA. (e-mail: bingnan.li1@uga.edu, dl43052@uga.edu, yuan.ke@uga.edu). Yuan's research is partially supported by NSF-DMS-2210468.

monitoring RR [1] and IBI could be used for heart rate variability (HRV) analysis which contributes not only to atrial fibrillation [2] but also stress analysis [3], [4]. Recently, wearable devices, such as Apple watch [5] and Garmin heart rate monitors [6], have been developed for HR [1], [7] and RR [8], [9] monitoring. However, they are intrusive [10] as they require continuous body contact to monitor vital signs. Many elderly people feel uncomfortable or sometimes forget to wear these devices and children may accidentally lose them. In addition, wearable devices can cause skin irritation for infants [11]. Thus, the contactless technique is a potential solution for a sleep monitoring system to address those problems since there is no need to wear an external device [10].

In this paper, we introduce a novel real-time contactless sleep monitoring system, named BedDot. BedDot aims to monitor sleep and vital signs in a contactless manner which could be easily applied in both the home environment and hospital environment. The installation and the BedDot device are illustrated in figure 1. BedDot is composed of a Raspberry Pi as the onboard computer, an Analog Digital Convert (ADC) board, and a vertical geophone as a vibration detector. The key component of BedDot is the geophone sensor that collects real-time signals to measure micro-vibrations produced by the cardiac activity of humans. It is highly sensitive to micro-vibrations and can be used to detect earthquakes [12]. When we install a BedDot under the mattress/seat, the geophone is capable of detecting micro-vibrations created by heart beat [13].

Most existing contactless systems, e.g. [14]–[17] require a specific mattress or cushion and expect the heart to position vertically above the device to capture vital signs. For radar-based devices, continuous monitoring would mean continuous radiation, which is a health concern for some people. There is no radiation, no specific distances setting and orientation setting for BedDot compare to radar-based system [18]–[21]. And it is easy to install a BedDot under the bed/seat for monitoring vital signs compare to either pressure sensors or radar-based devices. Furthermore, most existing works focus on how to estimate vital signs on processed and cleaned signals. However, how to obtain high-quality data to avoid giving unstable results caused by low-quality data is still under-explored. There is no existing work on how to automatically obtain signals for accurate vital signs estimation in a contactless manner during sleep in real-time. To the best of our knowledge, we are the first ones to integrate a

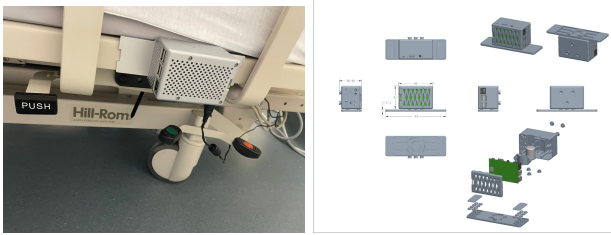


Fig. 1: Installation of BedDot on the side of bed frame(left), BedDot device(right).

signal quality assessment algorithm in a contactless sensing system for real-time vital signs estimation(HR, RR, and IBI) of sleep. Specifically, our signal quality assessment algorithm consists of three parts: bed occupancy detection, movement detection, and heartbeat detection. For bed occupancy, most of the existing work focuses on detecting the 'moment of the person on the bed(bed entry)' and 'the moment of person off the bed(bed exit)'. However, simply detecting the bed entry and bed exit could lead to huge errors if false detection exists even once. For example, if a bed entry is detected when there is no person lying on the bed, all bed occupancy status afterward would be considered as 'on the bed' which would lead to continuous false detection. And, there are very few contactless sleep sensing systems and maybe none for geophone-based systems that can estimate IBI, let alone estimate HR, RR, and IBI simultaneously. In addition, geophone-based RR estimation is very difficult as the vibration caused by respiration is not well recorded due to low frequency. RR estimation of previous geophone-based work is done by square-law amplitude demodulation algorithm [13] which assumes the respiration causes the amplitude fluctuation of the geophone signal. However, it didn't reveal the respiration pattern of the geophone signal very obviously based on most of our observations. Hence, geophone-based RR estimations are still under-explored.

Challenges of Bed Occupancy Detection: (1) the geophone has internal systematic errors as the outputs are not equal to zero due to environmental noises even if there is no person lying in bed. Hence, simply detecting bed occupancy by checking signal amplitude will fail. Although the signal energy of bed entries and bed exits is generally much larger than that of other types of signals, a big movement on the bed or an event off the bed caused by a huge vibration would lead to a false detection which would lead to cascade failures. (2) even if there is no person on the bed, some vibrations caused by events around the bed could lead to similar waveform properties as a heartbeat, such as vibrations caused by footsteps or other periodic vibrations.

Challenges of Heart rate estimation: The waveform of our collected heartbeat signal varies depending on multiple factors such as sensor location, types of beds, environmental noise, and different people, which leads to difficulties in accurately estimating heart rate (HR). In addition, some of our heartbeat signals show systolic peaks and diastolic peaks in one cardiac cycle, which could lead to an estimation result that is double the ground truth if peak detection algorithms are applied.

Challenges of RR Estimation: High-quality data can reveal a clearer heartbeat pattern, but detecting respiration patterns can be difficult with geophones because they are insensitive to low-frequency vibrations, making it challenging to estimate respiration rate (RR). The slow vibration speed caused by respiration is easily buried under noise and heartbeat patterns.

Challenges of IBI Estimation: Most of the time, the heartbeat peak of each cardiac cycle is buried within the noise, which makes it more challenging to accurately locate the heartbeat peak position for inter-beat interval estimation. Therefore, performing heartbeat peak detection directly on raw or denoised data results in poor performance.

The major contributions of this paper are summarized as follows:

- 1) To the best of our knowledge, we are the first to design an automatic signal quality assessment algorithm integrated into a sleep monitoring system to select high-quality data and avoid undesirable results for further HR, RR, and IBI estimation.
- 2) We introduce a Bayesian theorem strategy to fuse features and estimate HR and RR. We extensively test this approach on 75 individuals with diverse conditions to demonstrate the generalizability of our algorithms.
- 3) We introduce a RR estimation algorithm that reconstructs the waveform of the respiration signal from the heartbeat signal. We present a series of mathematical formulations of the problem from a different perspective compared to previous geophone-base systems. And the algorithm is shown to perform well in real world datasets.
- 4) Our system is adaptable from bed to seat, and we achieved good performance on HR, RR, and IBI estimation for 16 individuals on a seat. To the best of our knowledge, we are the first to introduce a geophone-based system capable of calculating RR on a seat and IBI for both seats and beds.

The rest of the paper is organized as follows. Section II reviews the related works of bed occupancy detection, and contactless vital signs monitoring. Section III presents the Methodology of our system, bed occupancy detection, movement detection, HR, RR and IBI estimation. Section IV introduces the process of experiment setup and system visualization, then reports the evaluation results. Finally, we conclude this paper in section V.

II. RELATED WORKS

A. Bed Occupancy Detection

[22]–[24] calculated a baseline threshold when no one is on bed as the prior knowledge. Then, the calculated threshold is used to compare with incoming signals to determine the bed occupancy status. This type of methods are easy and intuitive. However, there is no statistical result for this method on those references which makes it hard to evaluate the performance. In addition, it needs to be re-initialized each time with a different environment.

[25] proposed a feature fusion method by combining Spectral Entropy, Kurtosis and Teager Energy Operator (TEO) to

recognize bed entry and bed exit. They achieved high accuracy on their dataset. However, they only detect moment of 'bed entry' and 'bed exit' instead of continuously detecting 'on bed' or 'off bed' status, that potentially could bring continuous errors if one moment of 'bed entry' and 'bed exit' has been falsely detected.

[10] using an autocorrelation function to detect if the signal is periodic to differentiate 'on bed' and 'off bed' signals. This method could achieve very high accuracy. However, when another periodic signal other than a heartbeat exists it could lead to false detection.

B. Contactless Vital Sign Estimation

Contactless sleep monitoring for vital signs has been a very hot topic in recent years. For example, the authors of [18] use two radio devices to receive the reflected signal from the human body and apply a fast Fourier transform (FFT) to transform the signal from the time domain to the frequency domain. Afterward, they performed FFT denoising to simulate a bandpass filter on the frequency domain. Furthermore, they perform inverse FFT on the filtered frequency domain to recover a smoothed signal on the time domain. Finally, they estimate HR and RR by counting peaks in the filtered data. The authors of [19] use Doppler Radar and microwave signals to detect air vibrations caused by heartbeat and respiration. They apply bandpass filter signals with different frequency range cutoffs. Then, they perform FFT on filtered signals to estimate HR and RR. Their methods are simple to implement, but not applicable to signals with complicated waveforms.

The authors of [26] proposed a near-infrared (NIR) camera-based sleep monitoring system. They extract pulse signals from continuous NIR frames by a PBV algorithm [27] and perform FFT on the extracted signal to get pulse rates. However, their system can not estimate RR. In addition, the camera-based system may cause privacy violation issues which should also be taken into consideration.

[14]–[17] require a special mattress with integrated sensors to collect ballistocardiography (BCG) to estimate HR and RR. [28] uses load cells and [29], [30] uses Electromechanical film sensors to monitor HR and RR which are cumbersome to install. [31] propose an Inter-beat interval algorithm based on segment correlation of signal which requires post-correction. [32] also propose a robust inter-beat interval estimation algorithm which has been adopted a lot in literature and commonly set as a baseline method. However, their method has to divide a signal into many segments and apply convolution operation on each segment which requires much more computational cost, that may not be suitable for a real-time system.

Previous geophone-based system [12] uses a geophone to capture vibration signals caused by heart movements. For HR estimation, they first perform a low pass filter to separate the noise and heartbeat data. Then, they adopt a peak finding algorithm [33] on the autocorrelation function (ACF) of the raw signal to estimate HR. In their follow-up work [13], they developed an RR estimation algorithm based on the square-law amplitude demodulation. They perform peak detection on ACF of denoised data instead of raw signal

could lead to prominent heartbeat peaks compared to either raw data or denoised data. However, ACF on denoised data directly could generate many small peaks, most of which are not heartbeat peaks. Hence, this could degrade the performance of the peak detection algorithm which gives unstable results. In addition, the peak detection algorithm needs a threshold for peak detection which is difficult to select an optimal one because of various waveforms. And, although, they analyze RR based on square-law amplitude demodulation, the main idea is to apply a low pass filter and combine it with FFT, which is simple but not stable. Plus, performance is not good enough.

Another geophone-based system [25] uses a band-pass filter first and they extract the envelope by detecting peaks and then connecting them to form an envelope. Next, they detect the local maxima of the envelope and set a threshold to eliminate outliers. Lastly, they take an average of detected peaks intervals to calculate HR. For RR estimation, they extract the RR envelope by connecting peaks on the HR envelope using interpolating. Their method is easy to implement and intuitive as they leverage envelope to estimate heart rate and respiration rate. However, this method of extracting the envelope has obvious boundary issues at the start and end of the signal. Furthermore, peak detection on the envelope is not stable if the envelope is noisy such as having many small spikes which are impossible to eliminate.

All the works presented above does not discuss if the system is ready(bed/seat occupancy detection) to automatically obtain high-quality data(signal quality assessment) to avoid giving undesirable results and in the meanwhile estimate vital signs accurately.

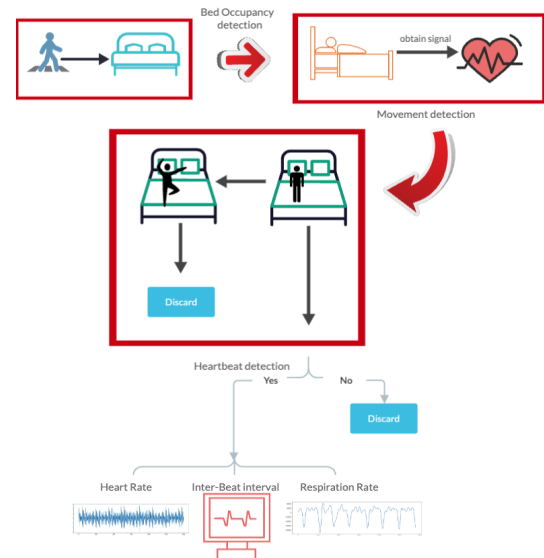


Fig. 2: Work flow of vital signs monitoring by BedDot.

III. METHODOLOGY

The workflow of the BedDot system is summarized in Figure 2. Raw data is collected by the geophone in BedDot, which is usually placed under the bed for human vital signs monitoring. In this section, we introduce the methods for signal quality assessment which consists of bed occupancy

detection, movement detection along with heartbeat detection, and HR estimation. Then, we introduce algorithms for RR and IBI estimation.

A. Signal Quality Assessment and Heart rate estimation

To ensure accurate estimation of HR, RR, and IBI from the seismic signal collected by BedDot, it is important to eliminate noise and other non-vital activity vibrations that may interfere with the signal. The signal is composed of various sources of vibration, including background white noise, home environment noise from appliances (such as air conditioners, washers, and dryers), body movements during sleep, and vibrations from vital activities such as heartbeat, respiration, and blood pressure changes. To eliminate non-vital activity vibrations, our algorithm first detects if there is a person on the bed. If so, it checks for any movement present in the signal. Finally, the signal is used for vital sign calculation only if it contains clear and detectable heartbeats. The detailed workflow of the signal quality assessment algorithm is shown in figure 3.

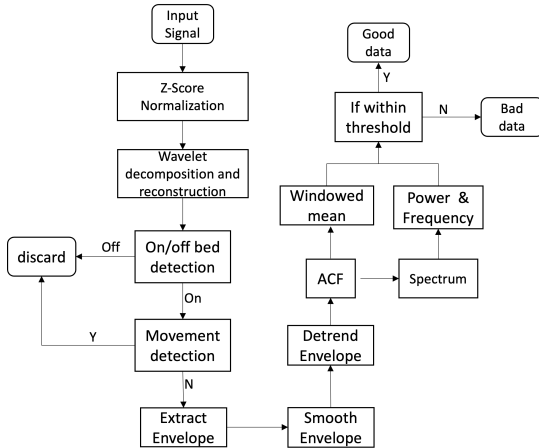


Fig. 3: Signal Quality Assessment Algorithm

1) Data Preprocessing: The z-score transformation is used to standardize signal x as $\tilde{x} = [x - \text{mean}(x)]/\text{std}(x)$ where $\text{mean}(x)$ and $\text{std}(x)$ stand for the mean and standard deviation of x . The signal collected by BedDot is generated by body mass movements caused by cardiac activity. To denoise this signal, we perform discrete wavelet decomposition. There are two reasons we choose wavelet denoise over a bandpass filter: (1) Wavelet denoise has fewer boundary issues compared to a bandpass filter with zero phase shift, and (2) a bandpass filter suppresses all out-of-band noise but does not denoise the passband signal. Wavelet denoise decomposes a noisy signal into different scales and removes noise while preserving the signal, regardless of the frequency content.

For wavelet denoise, Daubechies 12 (db12) has been selected as the mother wavelet because db12 is similar to the cardiac cycle of our collected signal. Discrete wavelet decomposition is to decompose the signal into different frequency ranges. The signals are passed through a low-pass filter $y_{\text{low}}[n] = \sum_{k=-\infty}^{\infty} x[k]l[2n-k]$ and a high-pass filter $y_{\text{high}}[n] = \sum_{k=-\infty}^{\infty} x[k]h[2n-k]$ simultaneously for each

decomposition. where $l(\cdot)$ stands for low pass filter, y_{low} is the decomposed low frequency signal, $h(\cdot)$ stands for high pass filter, y_{high} is the decomposed high frequency signal, and x is previous decomposed low frequency signal. For each decomposition, the frequencies of the signal have been divided in half. For example, if the frequency range of x is $[0, f]$, the frequencies have been split into a low frequency range $[0, 2/f]$ and a high frequency range $[2/f, f]$. The output of the low-pass filter is then further processed by passing it through a new low-pass filter and a new high-pass filter for further decomposition. Since our signal sampling rate is 100 Hz, based on the Nyquist–Shannon sampling theorem, the valid frequency range is up to 50 Hz. The signal has been decomposed six times to obtain seven components. The frequency ranges for the seven components (from D1 to D6 and A1) are $[25, 50]\text{Hz}$, $[12.5, 25]\text{Hz}$, $[6.25, 12.5]\text{Hz}$, $[3.125, 6.25]\text{Hz}$, $[1.5625, 3.125]\text{Hz}$, $[0.78125, 1.5625]\text{Hz}$, and $[0, 0.78125]\text{Hz}$, respectively. Finally, in this case, we select the decomposed components with frequency ranges from 0.8 Hz to 12 Hz (i.e., from D3 to D6) to reconstruct the denoised signal. An example of wavelet denoising is shown in figure 4.

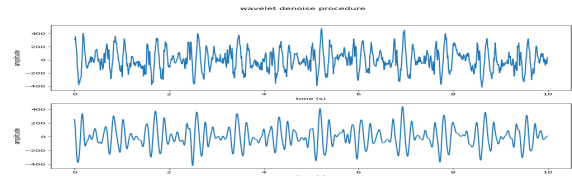


Fig. 4: Top row of the figure shows raw data while the bottom row of the figure shows the wavelet decomposition and reconstructed signal.

2) Bed Occupancy Detection: After wavelet decomposition and reconstruction of the raw data, we obtained a denoised signal. The first function of BedDot is to detect if the bed is occupied by a user, i.e., an on/off-bed detection algorithm. As we introduced in Section I, there are two main challenges for bed occupancy detection. First, the geophone has its own system errors, which makes it difficult to detect whether a person is on the bed based on amplitude directly. Additionally, simply detecting bed entry and bed exit based on signal energy could bring cascading failures. Second, there could be some other vibrations or interference during the 'on bed' and 'off bed' periods that would degrade the performance of bed occupancy detection.

To deal with the first challenge, we differentiate the 'on bed' signal from the 'off bed' signal by leveraging the difference between the waveforms of the two types of signals. Motivated by the speech detection problem in audio signal processing, we calculate the zero crossing rate of the denoised signal to distinguish the 'on bed' signal from the 'off bed' signal. The zero crossing rate is the rate at which a signal transitions from positive to negative and from negative to positive: $zcr = \frac{1}{N-1} \sum_{i=1}^{N-1} 1_{\mathbb{R}_{<0}}(x_i \cdot x_{i-1})$ where zcr stands for zero crossing rate, x is a signal with length N and $1_{\mathbb{R}_{<0}}$ is a indicator function. The zero crossing rate is frequently used to detect whether speech exists in an audio signal since the amplitude of a signal that contains speech would suddenly rise

up and oscillate less than the background noises. Therefore, the zero crossing rate of speech segments is much lower than that of the audio segments without speech. Hence, the zero crossing

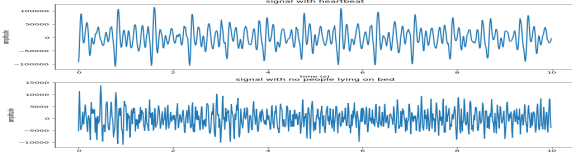


Fig. 5: The figure at the top shows the signal that contains the heartbeat. The figure at the bottom displays the signal with no person lying on the bed. It can be easily observed that the signal on the bottom fluctuates more.

rate (ZCR) can be considered an indicator of the shape of the waveform and can quantify the frequency of a signal in the time domain. We adopted this idea as the heartbeat signal could be considered as 'speech' when a person is lying on the bed, while the vibration signals created by the environment can be treated as 'background noise'. It is easy to observe that the signal that contains the heartbeat signal shows much less oscillation compared to the 'signal with no person lying on the bed' as shown in figure 5. Our experiment justified this conjecture as we observed that the zero crossing rate when a person is lying on the bed (on-bed) is indeed much lower than that of when no person is on the bed (off-bed). We demonstrate this finding by showing the zero crossing rate of about one week of sleep monitoring for one person in figure 6. The red rectangular in figure 6 shows the period of 'off bed', and the green rectangular shows the period of 'on bed'. It can be easily observed that the 'off bed' period shows a much higher zero crossing rate.



Fig. 6: 'Signal with no person lying on bed'(red rectangular) shows a higher zero crossing rate than 'signal with people lying on bed'(green rectangular)

To address the second challenge of distinguishing vibrations caused by footsteps or other environmental factors from signals with the heartbeat, we use the kinetic energy change between two consecutive time steps. This is based on the intuition that some events that cause vibration would suddenly change the waveform of the signal and induce many high spikes, which would lead to a huge change in the signal energy. In our algorithm, we first calculate the energy of the signal in each time step using the $e(T) = \frac{1}{2} \cdot m \cdot \sum_{t=T-N}^T v(t)^2$, where $e(T)$ is the kinetic energy for a segment of signal with length N , $v(t)$ is the measured velocity in time t , and m is the mass of the object. Then, we calculate the difference E_P between the energy of two consecutive time steps:

$$\begin{aligned} \Delta E_P(T_2) &= \frac{|e(T_2) - e(T_1)|}{e(T_1)} \\ &= \frac{\left| \sum_{t=T_2-N}^{T_2} v(t)^2 - \sum_{t=T_1-N}^{T_1} v(t)^2 \right|}{\sum_{t=T_1-N}^{T_1} v(t)^2}. \end{aligned} \quad (1)$$

We set a threshold value to differentiate between the energy changes caused by a person's heartbeat and those caused by footsteps or other environmental vibrations. If $\Delta E_P(T_2)$ is greater than the threshold we classify it as an external event; otherwise, we classify it as a heartbeat signal. Based on the empirical test of large data the threshold here is set as 20%. In summary, our algorithm for bed occupancy detection combines the use of zero crossing rate and energy change to accurately distinguish between signals with heartbeat and signals caused by external events. Then, we will decide the bed occupancy of 'event' signals based on the status of pre-event and post-event.

3) Movement Detection: Once we can successfully detect that the bed is occupied, we need to further assess the status of the person lying on the bed because their movements can distort the vibration signals collected by BedDot. The bottom of figure 8 shows a piece of signal that is affected by on bed movements. We observe that the movements on bed usually create large vibrations and hence more outliers in the collected signals, which lead to a huge difference on signal distribution compare to signals with no motion artifacts. We demonstrate this by showing the distributions of signals affected by movements and signals with a heartbeat in figure 7. We utilize this

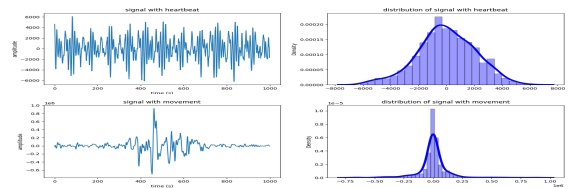


Fig. 7: Distributions for signals with heartbeats and signals with movements

observation and propose to use Kurtosis to detect if a piece of signal contains movements. Kurtosis measures the centered fourth moments of a distribution, which are commonly used as indicators for the existence of outliers and/or heavy-tailed errors. For a random sample $\{x_i\}_{i=1}^n$, the empirical Kurtosis of $\{x_i\}_{i=1}^n$ can be computed as $\kappa_x = \frac{\sum_{i=1}^n (x_i - \bar{x})^4}{ns^4}$, where \bar{x} and s are sample mean and standard deviation of $\{x_i\}_{i=1}^n$, respectively. When $\kappa_x > 3$, the empirical distribution of $\{x_i\}_{i=1}^n$ have tails heavier than Gaussian distribution. Thus, we use a large κ_x as strong evidence to detect movements in signals. In our case, we empirically select a threshold of 5 to detect if a signal contains movement when a person is sleeping.

4) Heartbeat Detection and HR estimation : Some signals recorded from the bed may not contain movement but still fail to show a clear heartbeat, as shown on the bottom row of figure 8. These types of signals should be removed to avoid inaccurate estimation of vital signs. After all the aforementioned quality assessment steps, if a signal is identified as good quality, then it is used to calculate HR, RR, and IBI. HR estimation is integrated with a heartbeat detection method. A key challenge of our HR estimation algorithm is the detailed shape of the waveform within each heartbeat cycle, which contains a lot of randomness and can be misleading for HR estimation. Thus, we use the envelope of the heartbeat cycle,

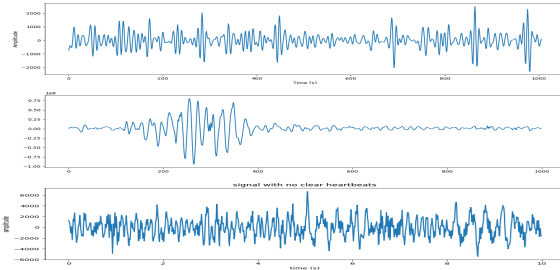


Fig. 8: Signal contains movement(foot step) caused by events around bed(top). Signal with people lying on bed but containing movement(middle).'On-bed' Signal with no clear heartbeat(bottom).

which is a smoothed counterpart of the waveform to calculate HR. Its periodicity is easier to detect because the noise is largely canceled out. With this motivation, we illustrate a signal processing procedure for HR estimation that consists of the following four steps. We also provide an example of this procedure in figure 9 to demonstrate its effectiveness.

Step 1. To extract the envelope of the signal, we use a Hilbert transform [34]. The Hilbert transform assumes that the amplitude of the signal is modulated by its instantaneous amplitude (envelope) according to the equation $x(t) = a(t) \cdot \cos(\omega t)$, where $x(t)$ is the raw signal and $a(t)$ is the envelope that we want to extract from $x(t)$. The Hilbert transform finds the imaginary part $x_i(t)$ of a real signal $x(t)$ as $x_i(t) = HT[x(t)]$, where $HT[\cdot]$ denotes the Hilbert transform operator. An analytic signal can be created from the real signal $x(t)$ and its Hilbert transform $x_i(t)$ as $z(t) = x(t) + i \cdot x_i(t)$. The envelope $a(t)$ can then be obtained as $a(t) = \sqrt{x^2(t) + x_i^2(t)}$.

Step 2. To further process the envelope of the signal, we apply a Savitzky–Golay filter [35]. The Savitzky–Golay filter is a polynomial filter based on least squares. It works by fitting a polynomial function to a small subset of adjacent data points and then using the coefficients of the polynomial to estimate the smoothed value of the central data point. This process is repeated for each data point in the signal, resulting in a smoothed version of the signal with reduced noise and sharper features. The spikes in the extracted envelope correspond to rapid changes in the amplitude of the signal, which can result from noise or artifacts in the original signal. By smoothing these spikes, the Savitzky–Golay filter helps to improve the accuracy of subsequent processing steps.

Step 3. To identify the periodicity of the smoothed envelope, we calculate its autocorrelation function (ACF) using a commonly used function in time series analysis. The ACF measures the correlation between the envelope at time t and the envelope at time $t+k$, and thus can reveal the periodicity of the signal: $ACF(k) = \frac{\sum_{i=1}^{n-k}(x_i - \bar{x})(x_{i+k} - \bar{x})}{\sum_{i=1}^n(x_i - \bar{x})^2}$. As we can see, $ACF(k)$ measures the lag- k autocorrelation within $\{x_i\}_{i=1}^n$. For a stationary periodic signal, the mean and variance are usually stable. To determine if the signal is periodic, we set a threshold based on the absolute value of the sample mean over a small window. If the absolute value of the sample mean is below the threshold, the signal is considered periodic.

Step 4. We analyze the frequency domain of ACF by

computing the power spectral density (PSD) using Welch's method [36]. Welch's method calculates a windowed PSD of overlapping segments of a signal. The average of all windowed PSDs is taken to make the final PSD smooth and robust. The windowed PSD is defined as the fast Fourier transformation (FFT) of a signal segment multiplied by a window function (i.e., Hamming function). The major frequency component of ACF should be between 0.7Hz and 3Hz, which is the normal heartbeat frequency range for humans. The magnitude of the maximum frequency peak should be larger than a pre-specified autocorrelation lower bound, such as 0.1, to distinguish the signal from random noises. We identify a piece of signal as containing a rich periodic signal for vital sign estimation if both the frequency and magnitude conditions are satisfied.

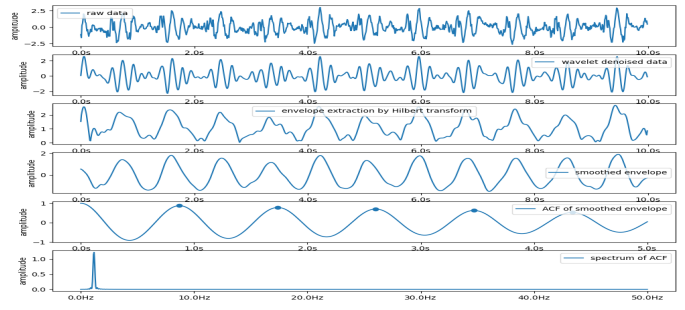


Fig. 9: Procedure for detecting heartbeat of the signal by obtaining ACF from a smoothed envelope of signal

Traditionally, HR is estimated by counting the number of heartbeats in a signal. However, this approach suffers from an instability issue in real-time monitoring setups. Suppose the true HR of a participant is 60 beats per minute (bpm). For a 10-second signal, a mis-calculation of one heartbeat may lead to an estimation error of more than 10% for HR. To avoid this problem, the median of heartbeat intervals could be used as a robust alternative to estimate HR. However, occasionally, we may observe that the incoming signal contains two peaks in one heartbeat cycle, as shown in figure 10. The first peak is called the systolic peak, and the second peak is called the diastolic peak. As both peaks can be visible on the ACF, this can lead to double-count errors, as the estimated HR is nearly double the true HR label. To correct this error, we should ignore the ACF peaks that reflect the autocorrelation between systolic and diastolic peaks within each heartbeat cycle, which usually have a higher than normal frequency. In practice, we only choose the highest peak of ACF between 0.5 seconds and 1.43 seconds and ignore the other peaks outside this range. The choice of this interval covers HR between 36 bpm and 120 bpm, which falls within the normal HR range during sleep.

Furthermore, we combine the frequency domain features of the smooth envelope obtained from Step 2 with the ACF, considering ACF as a time domain feature. We only select the region of interest of ACF, which is between 0.5 seconds and 1.43 seconds. The frequency domain features are obtained using Welch's method. Similar to the ACF, we only select the frequency range of interest, which is between 0.6 Hz

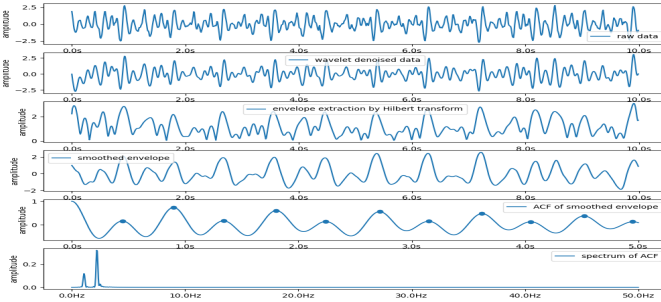


Fig. 10: Signal that contains 2 peaks within one heartbeat cycle

and 2 Hz. We convert these two features mentioned above into probability density functions (PDF) by applying softmax transformation on those two features: $\sigma(x_i) = \frac{e^{x_i}}{\sum_{j=1}^N e^{x_j}}$, where x_i is the i th data point in a segment signal x , $\sigma(\cdot)$ stands for softmax operation and N is the total number of data point in segment x . In order to combine the two features, we apply a probabilistic Bayesian theory. First, the spectrum obtained by Welch's method could be interpreted as 'the probability of the frequency (f) being the true fundamental frequency under the condition of the spectrum': $P(f|spectrum)$. ACF could be interpreted as 'the probability of a given number of data points(n) being the true periodicity under the condition of ACF': $P(n|ACF)$. Each feature gives a 'probability' of how likely it is for each possible input(f or n) to be the 'true'. Now, given the two independent PDFs, we aim to determine the most likely outputs under the combination of these two PDFs. We can replace f with n in $P(f|spectrum)$ as $n = \frac{Fs}{f}$ in order to form a joint distribution of $P(n|spectrum, ACF)$. Then, our goal here is to determine the most likely value of n under the combination of spectrum and ACF:

$$n = \arg \max_n P(n|spectrum, ACF). \quad (2)$$

According to Bayes' theorem, the joint distribution could be expressed as:

$$P(n|spectrum, ACF) = \frac{P(n) \cdot P(spectrum, ACF|n)}{P(spectrum, ACF)}, \quad (3)$$

where $P(spectrum, ACF)$ is a constant factor which do not depend on n and could be discarded later. And the likelihood of two features only depends on n and not on each other. Hence, equation (3) could be rewritten as:

$$P(n|spectrum, ACF) \propto P(n) \cdot P(ACF|n) \cdot P(spectrum|n). \quad (4)$$

We can apply the same operation on $P(ACF|n)$ and $P(spectrum|n)$. Then, the right side of equation (4) becomes:

$$\begin{aligned} & P(n) * P(ACF|n) * P(spectrum|n) \\ &= P(n) \cdot \frac{P(n|ACF) \cdot P(ACF)}{P(n)} \cdot \frac{P(n|spectrum) \cdot P(spectrum)}{P(n)} \\ &= P(n|ACF) \cdot P(ACF) \cdot \frac{P(n|spectrum) \cdot P(spectrum)}{P(n)}. \end{aligned} \quad (5)$$

$P(ACF)$ and $P(spectrum)$ could be dropped as they are not

depend on n . Therefore, equation (4) could be rewritten as

$$P(n|spectrum, ACF) \propto \frac{P(n|spectrum) \cdot P(n|ACF)}{P(n)}. \quad (6)$$

It is fair to assume $P(n)$ follows a uniform distribution since we do not give preference for any value of n . Then, $P(n)$ could be dropped as well. Finally, we get

$$P(n|spectrum, ACF) \propto P(n|spectrum) \cdot P(n|ACF). \quad (7)$$

Next, we can obtain 'true' n to be the most likely periodicity of the incoming signal by identifying the maximum output from the joint distribution of spectrum and ACF, $P(n|spectrum, ACF)$ according to equation (7). Denote F_s as the sampling rate of the signal and n as the 'true' periodicity with the highest probability. We propose to robustly estimate HR as $HR = \frac{60}{n} \cdot F_s$, where $n = \operatorname{argmax}_n(P(n|spectrum) * P(n|ACF))$.

B. IBI Estimation

Although IBI estimation is closely related to HR estimation, simply detecting peaks of the heartbeat will lead to a large number of false discoveries since the key step of IBI estimation is to locate every heartbeat peak position. However, locating heartbeat peaks on raw data or data after wavelet denoising may lead to enormous errors. In addition, our goal is to derive the interval between consecutive heartbeats. Hence, we care more about the difference between two consecutive peaks instead of the exact peak positions. In that sense, we propose to identify the peak positions on ACF instead and then estimate IBI as follows:

Step 1. We estimate the average IBI of the signal and locate the position of the first heartbeat peak (P_1) by finding the position of the peak with the maximum amplitude in the ACF of this signal within the range of $[0, N]$, where $N = IBI \cdot F_s$ is the number of data points for the average IBI.

Step 2. After locating the first heartbeat peak, we can adjust the start and end indices of the sliding window. The updated start index is $P_1 + 0.75 \cdot N$, and the updated end index is $P_1 + N + c$, where c is a small positive constant in case there is no heartbeat peak in the search window. Although rare, it is possible for some peak intervals to be larger than the average IBI within the given signal segment.

Step 3. We repeat Step 2 until the end index exceeds the length of the signal while ensuring that the start index remains within the signal length. After that, we check whether there are any remaining peaks in the signal. If we find any, we locate the position of the peak with the maximum amplitude. If not, we conclude that all heartbeat peaks have been detected.

Step 4. After all peaks of the heartbeat

$P = [p_1, p_2, \dots, p_i, \dots, p_N]$ have been detected, we then calculate IBIs for this signal segment as follows:
 $IBIs = [p_2 - p_1, \dots, p_i - p_{i-1}, \dots, p_N - p_{N-1}]$.

C. RR Estimation

It is difficult to identify a breathing cycle pattern from the raw signal, which is different from the heartbeat cycle.

We can see this difference on the first row of the signal in figure 11, which shows a 30-second signal. As we can observe, most heartbeats can be visually identified. However, it is much more challenging to identify any breathing cycles with our bare eyes. This is because the vibration velocity caused by respiration is much slower than the vibration velocity caused by heartbeat. The breathing cycle usually spans over multiple heartbeats and is not obvious in a short period of signals. It is intuitive to consider that displacement of the chest caused by breathing should be higher than a heartbeat. Hence, this motivates us to consider obtaining displacement data by applying integral over raw velocity data. By doing this, the respiration pattern could be revealed from raw data. However, the output of the geophone is not 'real' velocity, instead, it is almost proportional to velocity. In addition, the system of geophone has internal errors as it gives output value even if there are no vibration exists. Therefore, we formulate the output of geophone as follows:

$$x_i = C \cdot v_i + e_i, e_i \sim N(\mu, \sigma^2), \quad (8)$$

where x_i is the output of geophone in time-step i , v_i is the true velocity, C is an unknown factor as x_i is almost proportional to v_i and e_i is the internal error term which introduced by geophone follow a Gaussian distribution with mean equals to μ and variance equals to σ^2 . And the expectations of x_i are:

$$E[x_i] = C \cdot E[v_i] + E[e_i] = C \cdot E[v_i] + \mu, \quad (9)$$

where $E[\cdot]$ is the expectation operation. Then, after centering the data, we have signals with the mean of internal error equal to zero:

$$x_i - E[x_i] = C \cdot (v_i - E[v_i]) + (e_i - \mu). \quad (10)$$

After data being centered, we substitute $x_i - E[x_i]$, $v_i - E[v_i]$ and $e_i - \mu$, with \hat{x}_i , \hat{v}_i and \hat{e}_i respectively. Then, equation (10) becomes:

$$\hat{x}_i = C \cdot \hat{v}_i + \hat{e}_i, \hat{e}_i \sim N(0, \sigma^2). \quad (11)$$

As we do not care too much about the amplitude of the signal when it comes to RR estimation, instead, we pay more attention to the waveform of the signal. Therefore, C could be ignored in this case. Finally, we have $\hat{x}_i = \hat{v}_i + \hat{e}_i$. Next, We perform integral on \hat{x}_i in order to reveal respiration pattern:

$$D_T = \int_{i=1}^T \hat{x}_i = \int_{i=1}^T (\hat{v}_i + \hat{e}_i) = \int_{i=1}^T \hat{v}_i + \int_{i=1}^T \hat{e}_i, \\ D_T = \sum_{i=1}^T \hat{x}_i = \sum_{i=1}^T (\hat{v}_i + \hat{e}_i) = \sum_{i=1}^T \hat{v}_i + \sum_{i=1}^T \hat{e}_i, \quad (12)$$

where D_T is the displacement at time-step T . Then, we substitute $\sum_{i=1}^T \hat{v}_i$ and $\sum_{i=1}^T \hat{e}_i$ with y_T and b_T :

$$D_T = y_T + b_T, b_T \sim N(0, T \cdot \sigma^2), \quad (13)$$

where $y_T = hd_T + rd_T$, hd_T is heartbeat displacement at time T and rd_T is the respiration displacement at time T which is the target signal we want to recover:

$$D_T = hd_T + rd_T + b_T. \quad (14)$$

Although we can see from equation (13) that the variance of the internal error is increasing with time, the respiration pattern can still be revealed after performing the operations described above, as shown in figure 11. The breathing pattern is very obvious in the second row of figure 11, but there is baseline wandering due to the system error, so detrending is needed first. Furthermore, we leverage wavelet denoising to

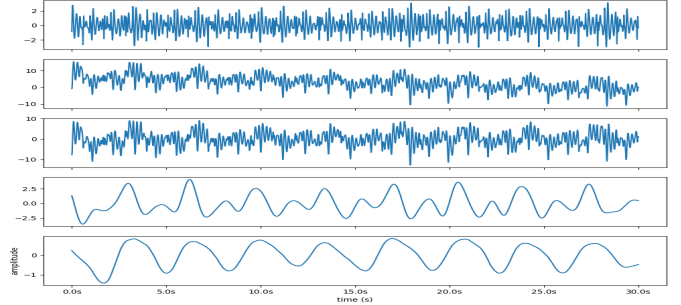


Fig. 11: (1) The first row is the raw data. (2) The second row is the respiration pattern revealed signal from raw data. (3) The third raw is detrended data from the second row. (4) The fourth row is wavelet denoised data from the third row. (5) The last row is data after removing the average of the fourth row.

filter out the interference of hd_T so that only the signals related to rd_T and b_T are left. In order to further recover rd_T , we apply a moving average filter with a relatively large window size. This is because $E[rd_T + b_T] = E[rd_T] + E[b_T] = E[rd_T]$. It is reasonable to assume that $E[rd_T] = rd_T$ under the assumption that the respiration signal is a deterministic signal. The entire procedure of recovering rd_T is shown in figure 11, and the bottom panel shows the final rd_T .

After obtaining the breathing signal rd_T , we calculate the ACF on the extracted signal. To further enhance the robustness of the RR estimation, we also adopt a similar feature fusion strategy as for HR estimation. We calculate the ACF on the wavelet denoised signal ($rr_{wav} = rd_T + b_T$), and the ACF on the detrended signal (third row in figure 11) after the Savitzky–Golay filter (rr_{sg}). This is because the breathing signal can sometimes be over-filtered, and rr_{sg} and $rr_{wavelet}$ may preserve a better shape compared to rd_T . Hence, we fuse all three features mentioned above to obtain a final probability density function (PDF) of the fused ACF as $P(n|ACF_{rd_T}, ACF_{rr_{wav}}, ACF_{rr_{sg}}) \propto P(n|ACF_{rd_T}) \cdot P(n|ACF_{rr_{wav}}) \cdot P(n|ACF_{rr_{sg}})$. Finally, we can estimate the respiratory rate (RR) by obtaining the maximum peak between 2 seconds and 10 seconds on the PDF of the fused ACF.

IV. EXPERIMENT SETUP AND EVALUATION

The BedDot device is shown in figure 1. BedDot can be easily attached using a magnetic mount to it. The cost of the system is affordable, and it can be easily deployed on a common bed or seat without any special alterations. During our experiments, we used a hospital bed and a seat in a hospital

environment, as well as a family bed in a home environment, to mimic real-world scenarios. Each bed had a BedDot attached underneath the chest area. For HR and RR labels, we used a commercially available FDA-approved Caretaker4 device as the reference. We collected data from 75 participants who were asked to lie in different positions such as on their back, stomach, right side, and left side. Afterward, participants were encouraged to nap to mimic real sleep. During the experiment, there were many movements caused by unintended body movements, intended changes of position, or other events around the bed/seat that could have buried the heartbeat in noise. The total dataset obtained after applying a signal quality assessment algorithm, which was able to estimate vital signs, contains 28,494 observations with no overlap between each data sample, collected from over 75 participants over 80 hours. To visualize the sleep status, we developed a graphical user interface (GUI) based on the Grafana tool [37], as shown in Figure 12. The upper panel displays the instantaneous HR and RR results, while the blue box in the top left corner indicates the bed's on/off status. The panel at the bottom shows the raw data collected from participants in real-time. This GUI also provides historical HR/RR data, body movement, posture changes, and bed status information. The system can be used for both online monitoring and offline post-analysis of historical data.



Fig. 12: Sleep monitoring GUI, that is able to visualize vital signs such as HR and RR.

For evaluation, we first compare the proposed vital signs estimation algorithms with a baseline method for HR, RR [12], [13], and IBI estimation [32]. For HR estimation and IBI estimation, we use 10-second segments of data for comparison and evaluation. For RR, we use 30-second, 20-second, and 10-second segment data to evaluate and compare, respectively. Then, we evaluate the bed occupancy result. Next, we evaluate HR, RR, IBI, and bed occupancy in different environments and conditions, including hospitals, homes, eds with different postures, and seats. Finally, we evaluate our signal quality assessment algorithm by comparing HR and RR performance on both datasets before and after applying the signal quality assessment algorithm. We report the Mean Absolute Error (MAE), the standard deviation of absolute error (STD), and the mean absolute error percentage (MAPE) for HR, RR, and IBI estimation. The mean absolute percentage error is defined as $MAPE = \frac{1}{n} \sum_{i=1}^n \left| \frac{\text{label}_i - \text{prediction}_i}{\text{label}_i} \right|$.

A. Comparison of HR, IBI, and RR estimation between the proposed algorithm and baseline method

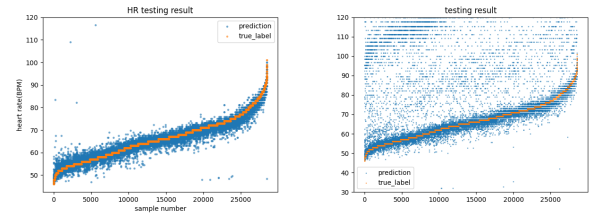


Fig. 13: HR estimation by the proposed algorithm (left) and baseline method (right) using 10-second data. The x-axis is the sample numbers. The y-axis is the HR (bpm) and the orange dots show the actual HR (in BPM) which are sorted in ascending order.

The results for HR estimation are presented in figure 13. From the figure, it is evident that our proposed algorithm is able to capture the trend of HR in prediction, but with a much lower variance of errors compared to the baseline algorithm. Most of the predictions of our proposed algorithm fall in the nearby area of true labels, which shows the stability of our HR estimation algorithm. The statistical results of the proposed HR estimation algorithm are shown in table I, which meets the AAMI standard (MAE within 5 BPM and MAPE within 10% for cardiac monitors and heart rate meters) [38]. Our proposed HR estimation algorithms outperform the baseline method in terms of MAE, STD, and MAPE.

TABLE I: Comparison between proposed algorithms and baseline methods on HR, IBI, and RR estimation with experiment data

METHOD	VITAL	MAE	MAPE	STD
PROPOSED ALGORITHM	HR(BPM)	1.08	0.0166	1.33
	10s RR(BPM)	2.05	0.1451	2.28
	20s RR(BPM)	1.80	0.1268	2.18
	30s RR(BPM)	1.54	0.1076	2.00
	IBI(ms)	24.81	0.0273	29.67
BASELINE METHOD	HR(BPM)	22.27	0.3509	36.84
	10s RR(BPM)	5.11	0.3630	4.61
	20s RR(BPM)	4.57	0.3074	4.52
	30s RR(BPM)	3.13	0.2149	3.40
	IBI(ms)	218.06	0.2532	402.59

Next, we evaluated the IBI results against the ground truth labels obtained from an FDA-approved device and compared them with the baseline method [32], since the previous geophone-based system was unable to provide IBI estimation [12], [13]. The results are shown in figure 14, which indicates that the proposed algorithm has much more stable results than the baseline method, as the prediction results are close to their corresponding true labels. Additionally, we report the statistical results of the IBI estimation in table I. The proposed IBI estimation algorithm outperforms the baseline method and achieves state-of-the-art performance in terms of MAE, MAPE, and standard deviation of error. Furthermore, the baseline method [32] takes much longer to process each data sample compared to the proposed algorithm.

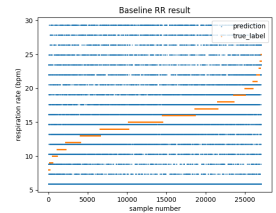
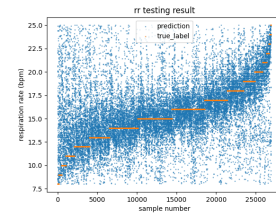
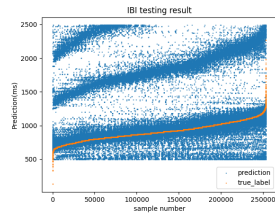
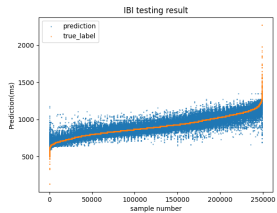


Fig. 14: IBI estimation by proposed algorithm(left) and Baseline method(right) using 10-seconds data. The orange dots represent the true IBI labels in ms sorted in ascending order, and the blue dots represent their corresponding predictions. The y-axis indicates the time interval of 2 consecutive heartbeats in ms.

The results for RR estimation using 10-second data, 20-second data, and 30-second data are presented in figures 15. In each figure, the ground truth of RR has been sorted in ascending order, as was done for HR evaluation, to demonstrate that the proposed methods can capture the trend with lower MAE compared to the baseline method. The results in table I show our proposed RR estimation algorithm outperforms the baseline RR estimation method in terms of MAE, STD, and MAPE on 10-second data, 20-second data, and 30-second data, respectively. For 30-second data, we achieved 1.54 ± 1.95 bpm (breaths per minute), and we also achieved good performance on 10-second segment data with a result of 2.18 ± 2.38 . There are almost no existing works that can use data less than 10 seconds to estimate RR. In contrast, the baseline method of RR estimation cannot learn any trend and performs poorly on 10s datasets. Although the baseline method could learn a trend on the 20s and 30s datasets, its performance is not as stable as ours.

B. Bed Occupancy Evaluation

The bed occupancy is evaluated based on accuracy, recall, specificity, and precision, with the confusion matrix shown in figure 16. Here, positive indicates 'on-bed', and negative indicates 'off-bed'.

Table II shows the achieved results for accuracy, sensitivity, specificity, precision, and recall, which are almost 100%. The bed occupancy detection results are given in real-time every second on a 10-second segment with a 30-second moving average window. The evaluation has been conducted on data collected from 75 people. Furthermore, we evaluated 10 days and nights of real scenarios on 10 people. Each day's data contains daily activities (with no sleep data but with daily events around the bed and background noise) and sleep.

TABLE II: Bed Occupancy Result Overall

Accuracy	Sensitivity (Recall)	Specificity	Precision
99.99%	99.99%	100%	100%

C. Evaluation on Different Environments

The previous sections have demonstrated that our algorithms can be generalized to different people. In this section, we evaluate the performance of our vital sign estimation and bed

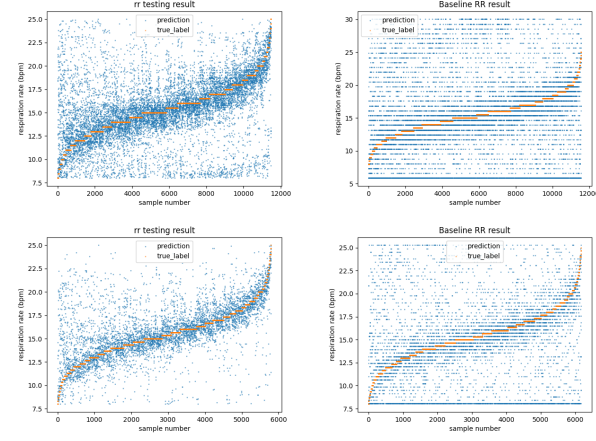


Fig. 15: RR estimation by the proposed algorithm(shown on the left of three rows) and baseline method (shown on the right of three rows). The y-axis is the RR (bpm). The orange dots show the actual RR (in BPM) sorted in ascending order and the blue dots are their corresponding predictions. 10 seconds data result to 30 seconds data results are shown from the top row to the bottom row.

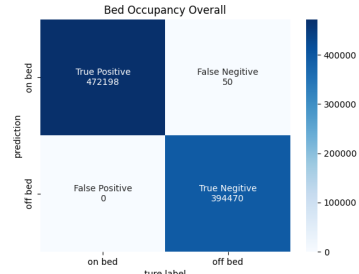


Fig. 16: Confusion Matrix of Bed Occupancy

occupancy algorithms in different environments, demonstrating their generalizability. Specifically, we evaluate the HR, RR, and IBI estimation and bed occupancy algorithms in home and hospital environments, respectively. Furthermore, we test and evaluate the HR, RR, and IBI estimation algorithms on a seat, demonstrating potential applications in smart offices.

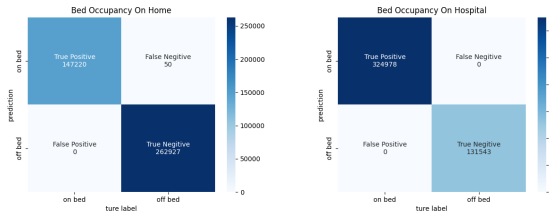
1) HR, RR, and IBI estimation on Different Environments and Seat: In this subsection, we evaluate the vital sign estimation algorithms on a hospital bed, a family bed, and a chair/seat to verify the generalizability of our algorithms. The results are shown in table III. For IBI estimation, the result on the hospital bed is slightly better than the result on the family bed, while for HR and RR estimation, the performance on the family bed is better compared to the hospital bed and seat. Overall, the performance of vital signs estimation is good across all conditions, which shows the generalizability of our algorithm

TABLE III: HR, RR, and IBI estimation on different conditions

CONDITIONS	VITAL	MAE	MAPE	STD
HOME	HR(BPM)	1.03	0.0161	1.17
	10s RR(BPM)	1.94	0.1357	2.14
	20s RR(BPM)	1.57	0.1099	1.81
	30s RR(BPM)	1.34	0.0930	1.65
	IBI(ms)	25.98(ms)	0.0283	31.39
HOSPITAL	HR(BPM)	1.17	0.0192	1.35
	10s RR(BPM)	2.61	0.1886	2.71
	20s RR(BPM)	2.17	0.1551	2.35
	30s RR(BPM)	2.02	0.1433	2.33
	IBI(ms)	22.88(ms)	0.0255	26.46
SEAT	HR(BPM)	1.03	0.0164	0.70
	10s RR(BPM)	2.86	0.2232	2.53
	20s RR(BPM)	2.27	0.1712	2.18
	30s RR(BPM)	1.43	0.1157	1.22
	IBI(ms)	30.18(ms)	0.0334	31.65

in different conditions.

2) *Bed Occupancy in Home Environment and Hospital Environment*: In this section, we evaluate the bed occupancy algorithm in different environments, namely home, and hospital, for 5 days each, respectively. The corresponding confusion matrices are shown in figure 17.

**Fig. 17:** Confusion Matrix of Bed Occupancy on Home(left) and Hospital(right)**TABLE IV:** Bed Occupancy Result on Different Environments

Environments	Accuracy	Sensitivity (Recall)	Specificity	Precision
Home	99.99%	99.97%	100%	100%
Hospital	100%	100%	100%	100%

The results of bed occupancy estimation in different environments are shown in table IV. As we can see from table IV, the false positive('on bed') appears more in home environment. And we check the period which appears false positive and we found that period contains the same characteristics as the heartbeat signal.

D. Evaluation of HR, RR and IBI estimation on Different Postures

In this section, we evaluate HR, RR, and IBI estimations on different postures, including lying on the back, left, right, and stomach. The evaluation results for different postures are shown in table V, which demonstrates that our vital signs algorithm can be adapted to all postures.

TABLE V: HR, RR and IBI estimation on different postures(lying on back, lying on right, lying on left and lying on stomach)

CONDITIONS	VITAL	MAE	MAPE	STD
BACK	HR(BPM)	1.03	0.0155	1.07
	10s RR(BPM)	2.17	0.1532	2.42
	20s RR(BPM)	2.01	0.1424	2.49
	30s RR(BPM)	1.83	0.1276	1.99
	IBI(ms)	26.31(ms)	0.0291	31.06
LEFT	HR(BPM)	1.00	0.0154	1.02
	10s RR(BPM)	1.80	0.1329	2.02
	20s RR(BPM)	1.84	0.1277	1.60
	30s RR(BPM)	1.60	0.1296	2.15
	IBI(ms)	25.30(ms)	0.0275	27.73
RIGHT	HR(BPM)	1.07	0.0154	1.07
	10s RR(BPM)	2.05	0.1501	2.32
	20s RR(BPM)	2.18	0.1601	2.16
	30s RR(BPM)	2.65	0.1801	2.81
	IBI(ms)	24.68(ms)	0.0298	33.12
STOMACH	HR(BPM)	1.19	0.0168	1.14
	10s RR(BPM)	2.50	0.1816	2.71
	20s RR(BPM)	1.93	0.1571	2.97
	30s RR(BPM)	1.21	0.0743	0.94
	IBI(ms)	21.25(ms)	0.0259	25.74

E. Evaluation for Effect of Signal Quality Assessment Algorithm

To assess the effectiveness of our signal quality assessment algorithm, we compared the HR and RR performance of our proposed algorithm on two datasets – one before and one after applying the signal quality assessment algorithm. Table VI presents the results obtained before applying the signal quality assessment algorithm. The performance of HR and RR estimation was found to be suboptimal prior to the application of our algorithm(shown in table I). However, after applying our signal quality assessment algorithm, we observed significant improvements in both accuracy and stability, as demonstrated by lower MAE, MAPE, and STD. Overall, these findings highlight the effectiveness of our algorithm in improving signal quality and facilitating more accurate HR and RR estimation.

TABLE VI: performance metrics for HR and RR estimation before applying our algorithm, while the comparison with performance after applying our algorithm is shown in () .

VITAL	MAE	MAPE	STD
HR(BPM)	5.46(\uparrow 4.38)	0.0795(\uparrow 0.0629)	9.71(\uparrow 8.38)
10s RR(BPM)	2.61(\uparrow 0.56)	0.1848(\uparrow 0.0397)	2.74(\uparrow 0.46)
20s RR(BPM)	2.56(\uparrow 0.76)	0.1801(\uparrow 0.0533)	2.76(\uparrow 0.58)
30s RR(BPM)	2.50(\uparrow 0.96)	0.1758(\uparrow 0.0682)	2.76(\uparrow 0.76)

V. CONCLUSION

In this paper, we introduce BedDot, a contactless bedside system that enables real-time monitoring of HR, RR, and IBI, as well as accurate bed occupancy detection during sleep. Our experiments demonstrate that BedDot performs well under varying conditions. Our device is cost-effective, easy to install, and allows for real-time visualization of vital signs and bed

occupancy status via our GUI design. Our proposed signal quality assessment algorithm can detect bed occupancy and filter out distorted signals without clear heartbeats, thereby improving the performance of vital signs estimation. Our vital sign estimation algorithms perform well, as evidenced by their MAE, std, and MAPE values, and their generalizability across various conditions. Our system has the potential to be commercialized as a clinical medical device or smart home device. In the future, we plan to extend our work to include AF detection and stress analysis, as well as expand our system's monitoring capabilities beyond in-bed sleep to include seat monitoring during daily activities.

REFERENCES

- [1] R. N. Aurora, S. P. Patil, and N. M. Punjabi, "Portable sleep monitoring for diagnosing sleep apnea in hospitalized patients with heart failure," *Chest*, vol. 154, no. 1, pp. 91–98, 2018.
- [2] A. A. Khan, G. Y. Lip, and A. Shantsila, "Heart rate variability in atrial fibrillation: The balance between sympathetic and parasympathetic nervous system," *European journal of clinical investigation*, vol. 49, no. 11, p. e13174, 2019.
- [3] H.-G. Kim, E.-J. Cheon, D.-S. Bai, Y. H. Lee, and B.-H. Koo, "Stress and heart rate variability: A meta-analysis and review of the literature," *Psychiatry investigation*, vol. 15, no. 3, p. 235, 2018.
- [4] Á. Jobbág, M. Majnár, L. K. Tóth, and P. Nagy, "Hrv-based stress level assessment using very short recordings," *Periodica polytechnica Electrical engineering and computer science*, vol. 61, no. 3, pp. 238–245, 2017.
- [5] Health on Apple Watch, "AppleWatch," 2018. [Online]. Available: <https://www.apple.com/healthcare/apple-watch/>
- [6] Garmin, "Garmin Heart Rate Monitors," 2018. [Online]. Available: <https://www.garmin.com/en-US/c/heart-rate-monitors/>
- [7] C. Paradiso, F. Colino, and S. Liu, "The validity and reliability of the mi band wearable device for measuring steps and heart rate," *International Journal of Exercise Science*, vol. 13, no. 4, p. 689, 2020.
- [8] B. Fang, N. D. Lane, M. Zhang, A. Boran, and F. Kawsar, "Bodyscan: Enabling radio-based sensing on wearable devices for contactless activity and vital sign monitoring," in *Proceedings of the 14th annual international conference on mobile systems, applications, and services*, 2016, pp. 97–110.
- [9] T. Hao, C. Bi, G. Xing, R. Chan, and L. Tu, "Mindfulwatch: A smartwatch-based system for real-time respiration monitoring during meditation," *Proceedings of the ACM on Interactive, Mobile, Wearable and Ubiquitous Technologies*, vol. 1, no. 3, pp. 1–19, 2017.
- [10] F. Li, M. Valero, J. Clemente, Z. Tse, and W. Song, "Smart sleep monitoring system via passively sensing human vibration signals," *IEEE Sensors Journal*, vol. 21, no. 13, pp. 14466–14473, 2020.
- [11] F. Adib, H. Mao, Z. Kabelac, D. Katabil, and R. C. Miller, "Smart homes that monitor breathing and heart rate," in *Proceedings of the 33rd annual ACM conference on human factors in computing systems*, 2015, pp. 837–846.
- [12] Z. Jia, M. Alaziz, X. Chi, R. E. Howard, Y. Zhang, P. Zhang, W. Trappe, A. Sivasubramanian, and N. An, "Hb-phone: a bed-mounted geophone-based heartbeat monitoring system," in *2016 15th ACM/IEEE International Conference on Information Processing in Sensor Networks (IPSN)*. IEEE, 2016, pp. 1–12.
- [13] Z. Jia, A. Bonde, S. Li, C. Xu, J. Wang, Y. Zhang, R. E. Howard, and P. Zhang, "Monitoring a person's heart rate and respiratory rate on a shared bed using geophones," in *Proceedings of the 15th ACM Conference on Embedded Network Sensor Systems*, 2017, pp. 1–14.
- [14] I. Sadek, E. Seet, J. Biswas, B. Abdulrazak, and M. Mokhtari, "Non-intrusive vital signs monitoring for sleep apnea patients: a preliminary study," *IEEE Access*, vol. 6, pp. 2506–2514, 2017.
- [15] J. H. Shin, Y. J. Chee, D.-U. Jeong, and K. S. Park, "Nonconstrained sleep monitoring system and algorithms using air-mattress with balancing tube method," *IEEE transactions on information technology in biomedicine*, vol. 14, no. 1, pp. 147–156, 2009.
- [16] Y. Zhu, J. Maniyeri, V. F. S. Fook, and H. Zhang, "Estimating respiratory rate from fbg optical sensors by using signal quality measurement," in *2015 37th annual international conference of the IEEE engineering in medicine and biology society (EMBC)*. IEEE, 2015, pp. 853–856.
- [17] M. Krej, Ł. Dziuda, and F. W. Skibniewski, "A method of detecting heartbeat locations in the ballistocardiographic signal from the fiber-optic vital signs sensor," *IEEE journal of biomedical and health informatics*, vol. 19, no. 4, pp. 1443–1450, 2015.
- [18] Z. Yang, P. H. Pathak, Y. Zeng, X. Liran, and P. Mohapatra, "Vital sign and sleep monitoring using millimeter wave," *ACM Transactions on Sensor Networks (TOSN)*, vol. 13, no. 2, pp. 1–32, 2017.
- [19] T. Rahman, A. T. Adams, R. V. Ravichandran, M. Zhang, S. N. Patel, J. A. Kientz, and T. Choudhury, "Dopplesleep: A contactless unobtrusive sleep sensing system using short-range doppler radar," in *Proceedings of the 2015 ACM International Joint Conference on Pervasive and Ubiquitous Computing*, 2015, pp. 39–50.
- [20] J. Liu, Y. Chen, Y. Wang, X. Chen, J. Cheng, and J. Yang, "Monitoring vital signs and postures during sleep using wifi signals," *IEEE Internet of Things Journal*, vol. 5, no. 3, pp. 2071–2084, 2018.
- [21] Y. S. Lee, P. N. Pathirana, T. Caelli, and R. Evans, "Doppler radar in respiratory monitoring: Detection and analysis," in *2013 International Conference on Control, Automation and Information Sciences (ICCAIS)*. IEEE, 2013, pp. 224–228.
- [22] M. Pouliot, V. Joshi, R. Goubran, and F. Knoefel, "Bed occupancy monitoring: Data processing and clinician user interface design," in *2012 Annual International Conference of the IEEE Engineering in Medicine and Biology Society*. IEEE, 2012, pp. 5810–5814.
- [23] M. Taylor, T. Grant, F. Knoefel, and R. Goubran, "Bed occupancy measurements using under mattress pressure sensors for long term monitoring of community-dwelling older adults," in *2013 IEEE International Symposium on Medical Measurements and Applications (MeMeA)*. IEEE, 2013, pp. 130–134.
- [24] A. Braun, M. Majewski, R. Wichert, and A. Kuijper, "Investigating low-cost wireless occupancy sensors for beds," in *Distributed, Ambient and Pervasive Interactions: 4th International Conference, DAPI 2016, Held as Part of HCI International 2016, Toronto, ON, Canada, July 17–22, 2016, Proceedings 4*. Springer, 2016, pp. 26–34.
- [25] J. Clemente, M. Valero, F. Li, C. Wang, and W. Song, "Helena: Real-time contact-free monitoring of sleep activities and events around the bed," in *2020 IEEE International Conference on Pervasive Computing and Communications (PerCom)*. IEEE, 2020, pp. 1–10.
- [26] T. Vogels, M. Van Gastel, W. Wang, and G. De Haan, "Fully-automatic camera-based pulse-oximetry during sleep," in *Proceedings of the IEEE Conference on Computer Vision and Pattern Recognition Workshops*, 2018, pp. 1349–1357.
- [27] G. De Haan and A. Van Leest, "Improved motion robustness of remote-ppg by using the blood volume pulse signature," *Physiological measurement*, vol. 35, no. 9, p. 1913, 2014.
- [28] A. Albukhari, F. Lima, and U. Mescheder, "Bed-embedded heart and respiration rates detection by longitudinal ballistocardiography and pattern recognition," *Sensors*, vol. 19, no. 6, p. 1451, 2019.
- [29] D. Friedrich, X. L. Aubert, H. Führ, and A. Brauers, "Heart rate estimation on a beat-to-beat basis via ballistocardiography-a hybrid approach," in *2010 Annual International Conference of the IEEE Engineering in Medicine and Biology*. IEEE, 2010, pp. 4048–4051.
- [30] J. M. Kortelainen and J. Virkkala, "Fft averaging of multichannel bkg signals from bed mattress sensor to improve estimation of heart beat interval," in *2007 29th annual international conference of the IEEE engineering in medicine and biology society*. IEEE, 2007, pp. 6685–6688.
- [31] A. Vehkaoja, S. Rajala, P. Kumpulainen, and J. Lekkala, "Correlation approach for the detection of the heartbeat intervals using force sensors placed under the bed posts," *Journal of medical engineering & technology*, vol. 37, no. 5, pp. 327–333, 2013.
- [32] C. Brüser, S. Winter, and S. Leonhardt, "Robust inter-beat interval estimation in cardiac vibration signals," *Physiological measurement*, vol. 34, no. 2, p. 123, 2013.
- [33] Tom O'Haver, "Peak finding and measurement," 2018.
- [34] M. Klingspor, "Hilbert transform: Mathematical theory and applications to signal processing," 2015.
- [35] A. Savitzky and M. J. Golay, "Smoothing and differentiation of data by simplified least squares procedures," *Analytical chemistry*, vol. 36, no. 8, pp. 1627–1639, 1964.
- [36] P. Welch, "The use of fast fourier transform for the estimation of power spectra: a method based on time averaging over short, modified periodograms," *IEEE Transactions on audio and electroacoustics*, vol. 15, no. 2, pp. 70–73, 1967.
- [37] Grafana Labs, "Grafana," 2018. [Online]. Available: <https://grafana.com/>
- [38] AAMI, "Cardiac monitors, heart rate meters, and alarms," 2023.